

# Dynamical Evolution and Spatial Mixing of Multiple Population Globular Clusters

Enrico Vesperini<sup>1</sup>, Stephen L.W. McMillan<sup>2</sup>, Francesca D’Antona<sup>3</sup>, Annibale D’Ercole<sup>4</sup>

<sup>1</sup>*Department of Astronomy, Indiana University, Bloomington, IN 47405, USA*

<sup>2</sup>*Department of Physics, Drexel University, Philadelphia, PA 19104, USA*

<sup>3</sup>*INAF- Osservatorio Astronomico di Roma, via di Frascati 33, I-00040 Monteporzio (Italy)*

<sup>4</sup>*INAF- Osservatorio Astronomico di Bologna, via Ranzani 1, I-40127 BOLOGNA*

8 March 2022

## ABSTRACT

Numerous spectroscopic and photometric observational studies have provided strong evidence for the widespread presence of multiple stellar populations in globular clusters. In this paper we study the long-term dynamical evolution of multiple-population clusters, focusing on the evolution of the spatial distributions of the first- (FG) and second-generation (SG) stars. In previous studies we have suggested that SG stars formed from the ejecta of FG AGB stars are expected initially to be concentrated in the cluster inner regions. Here, by means of  $N$ -body simulations, we explore the time scales and the dynamics of the spatial mixing of the FG and the SG populations and their dependence on the SG initial concentration.

Our simulations show that, as the evolution proceeds, the radial profile of the SG/FG number ratio,  $N_{SG}/N_{FG}$ , is characterized by three regions: 1) a flat inner part; 2) a declining part in which FG stars are increasingly dominant; and 3) an outer region where the  $N_{SG}/N_{FG}$  profile flattens again (the  $N_{SG}/N_{FG}$  profile may rise slightly again in the outermost cluster regions). Until mixing is complete and the  $N_{SG}/N_{FG}$  profile is flat over the entire cluster, the radial variation of  $N_{SG}/N_{FG}$  implies that the fraction of SG stars determined by observations covering a limited range of radial distances is not, in general, equal to the SG global fraction,  $(N_{SG}/N_{FG})_{glob}$ . The distance at which  $N_{SG}/N_{FG}$  equals  $(N_{SG}/N_{FG})_{glob}$  is approximately between 1 and 2 cluster half-mass radii. The time scale for complete mixing depends on the SG initial concentration, but in all cases complete mixing is expected only for clusters in advanced evolutionary phases, having lost at least 60–70 percent of their mass due to two-body relaxation (in addition to the early FG loss due to the cluster expansion triggered by SNII ejecta and gas expulsion). The results of our simulations suggest that in many Galactic globular clusters the SG should still be more spatially concentrated than the FG.

**Key words:** globular clusters:general, stars:chemically peculiar, methods:N-body simulations

## 1 INTRODUCTION

An increasing number of spectroscopic and photometric observational studies have provided strong evidence for a widespread presence of multiple stellar populations in globular clusters. The observed star-to-star variations of light elements, such as Na, O, Al, and Mg, indicates that a significant fraction (50–80%) of globular cluster stars must have formed out of matter processed through a high-temperature CNO cycle in a first generation of stars (hereafter FG; see e.g. Carretta et al. 2009a, 2009b and references therein). Photometric studies, by revealing the presence of multiple main sequences, subgiant, and red-giant branches in numer-

ous clusters, have buttressed the spectroscopic evidence and added important new elements to the observational framework of multiple population in globular clusters. In particular, photometric measurements have shown that some clusters host a population of very He-rich stars among the second-generation (hereafter SG) population of some clusters (see e.g. Piotto et al. 2007; see also D’Antona et al. 2002, D’Antona & Caloi 2004, D’Antona & Caloi 2008). Recently, the first direct measurement of He abundances of two stars in NGC 2808 has confirmed the strong He-enhancement suggested by those photometric studies (Pasquini et al. 2011; see also Dupree et al. 2011 for evidence of He enhancement in  $\omega$  Cen stars).

Models for the source of polluted gas from which SG stars formed include AGB stars (see e.g. Cottrell & Da Costa 1981, Ventura et al. 2001), rapidly rotating massive stars (Decressin et al. 2007), and massive binary stars (De Mink et al. 2009). A few studies have also explored some aspects of cluster formation and evolution for some of these models (see e.g. D’Ercole et al. 2008, 2010, 2012, Bekki 2011, Decressin et al. 2008, 2010; see Renzini 2008 and Gratton et al. 2012 and references therein for a review).

In D’Ercole et al. (2008), we focused our attention on the AGB model and explored the formation and dynamical evolution of multiple populations by means of hydrodynamical and N-body simulations. Our simulations show that the AGB ejecta form a cooling flow and rapidly collect in the innermost regions of the cluster, forming a concentrated SG stellar subsystem (see also Bekki 2011). In order to form the number of SG stars observed today, the FG cluster must have been considerably more massive than it is now. The N-body simulations presented in D’Ercole et al. (2008) show that the early expansion triggered by the loss of mass in the form of SNII ejecta leads to a strong preferential loss of FG stars resulting in a cluster in which the number of SG stars is similar to (or even larger than) that of FG stars as observed in several Galactic globular clusters (see e.g. Carretta et al. 2009a, 2009b).

In subsequent papers we expanded the initial models presented in D’Ercole et al. (2008) to further explore the origin of the observed abundance patterns (D’Ercole et al. 2010, 2012), the connection between multiple population globular clusters and the Galactic stellar halo (Vesperini et al. 2010) and the implications for the disruption of FG and SG binary stars (Vesperini et al. 2011).

In this paper we focus our attention on the long-term dynamical evolution of the multiple-population cluster, starting immediately after the early evolutionary stages during which a large fraction of the FG population is lost. We emphasize that, throughout this paper, when we discuss cluster mass loss we are referring only to mass lost by the cluster during its long-term relaxation-driven evolution, not the early phase responsible for the loss of most of the initial FG population.

After the early loss of FG stars (e.g. at  $\approx 1 - 2$  Gyr for the simulations presented in D’Ercole et al. 2008), a multiple-population cluster will start its long-term evolution driven by two-body relaxation with a similar number of SG and FG stars but with the SG population still concentrated in the cluster inner regions. A number of observational studies (Bellini et al. 2009, Carretta et al. 2010a, Lardo et al. 2011, Kravtsov et al., 2010, 2011, Nataf et al. 2011, Johnson & Pilachowski 2012, Milone et al. 2012) have found that in several clusters SG stars are indeed preferentially located in the inner regions and retain some memory of the initial segregation of the SG population predicted by the models we presented in D’Ercole et al. (2008).

Understanding the dynamics of the spatial mixing, and specifically the extent to which memory of the initial SG segregation predicted by the formation models is retained after one Hubble time of relaxation-driven evolution, is an essential step to properly interpreting observational data, as well as testing the key elements of theoretical scenarios of cluster formation and evolution.

In this paper, by means of N-body simulations, we ex-

plore the structural evolution of multiple population clusters. We focus our attention on the spatial mixing of the SG and the FG populations, and the evolution of the relative spatial distribution of the SG and the FG stars. The structure of the paper is as follows: in Section 2 we describe the initial conditions of our N-body simulations; in Section 3 we present our results; and in Section 4 we discuss our results and summarize our main conclusions.

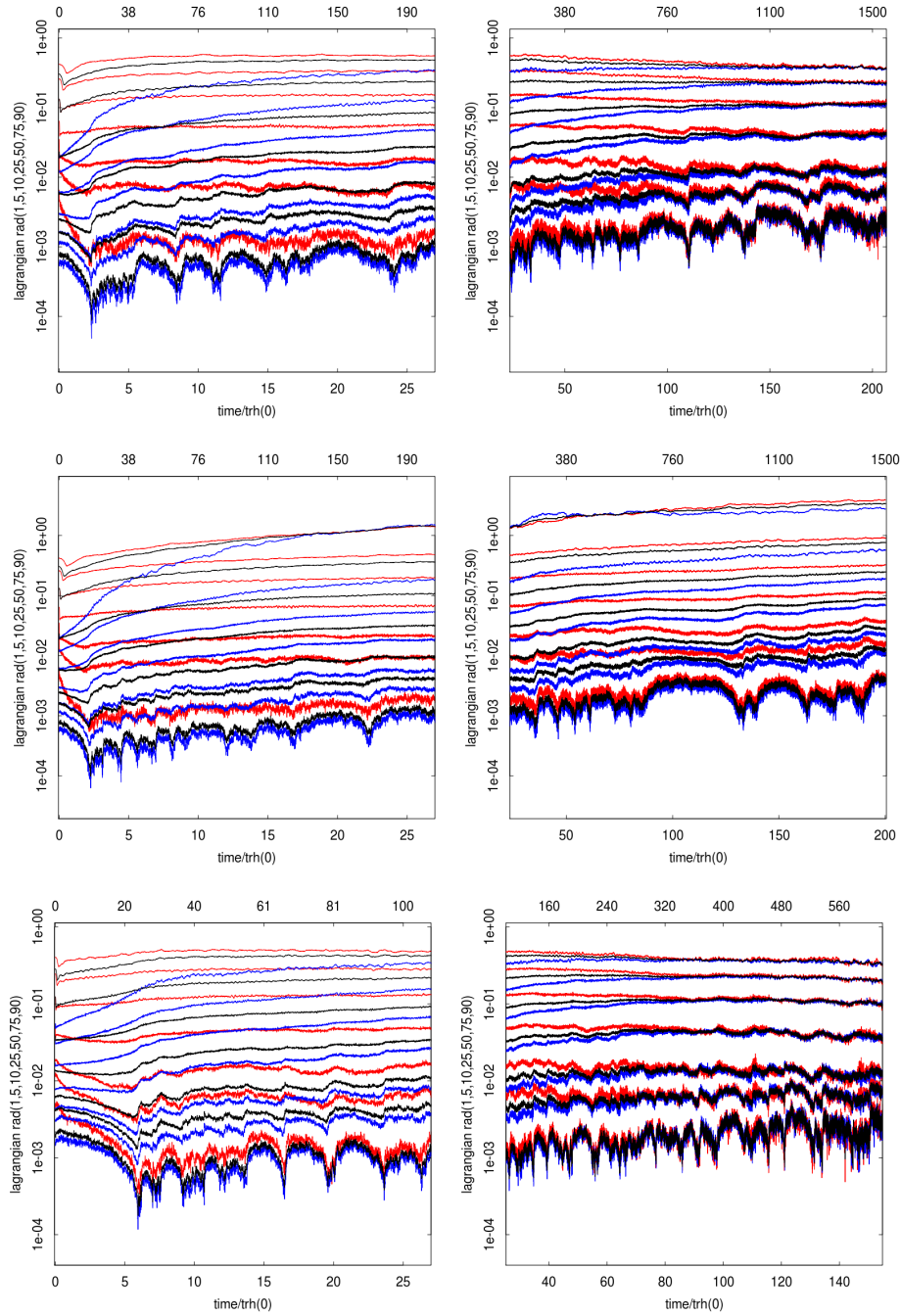
## 2 METHOD AND INITIAL CONDITIONS

The study presented in this paper is based on N-body simulations run with the `starlab` package (Portegies Zwart et al. 2001) and accelerated by GRAPE-6 special purpose hardware (Makino et al. 2003) and GPU (Gaburov et al. 2009). We explore the evolution of four systems with different degrees of initial concentration of the SG population. In all cases the initial conditions are set by simply combining two single-mass King (1966) models: the FG cluster is modeled as a King model with dimensionless central potential  $W_0 = 7$ ; the SG system is also modeled as a King model with  $W_0 = 7$ , but it is initially entirely contained within the inner regions of the FG system. Our models have an initial ratio of the FG to the SG half-mass radius,  $R_{h,FG}/R_{h,SG}$  equal to 2.5, 5, 10, and 25 ( $R_{h,FG}$  and  $R_{h,SG}$  are the 3D half-mass radii). Hereafter we refer to these simulations as *r2p5*, *r5*, *r10*, and *r25*. The models presented do not include primordial binaries or stellar evolution. The combined system is initially scaled to a virial ratio  $T/V = 0.5$  and is allowed to dynamically settle into an equilibrium state during the first few dynamical times of each simulation.

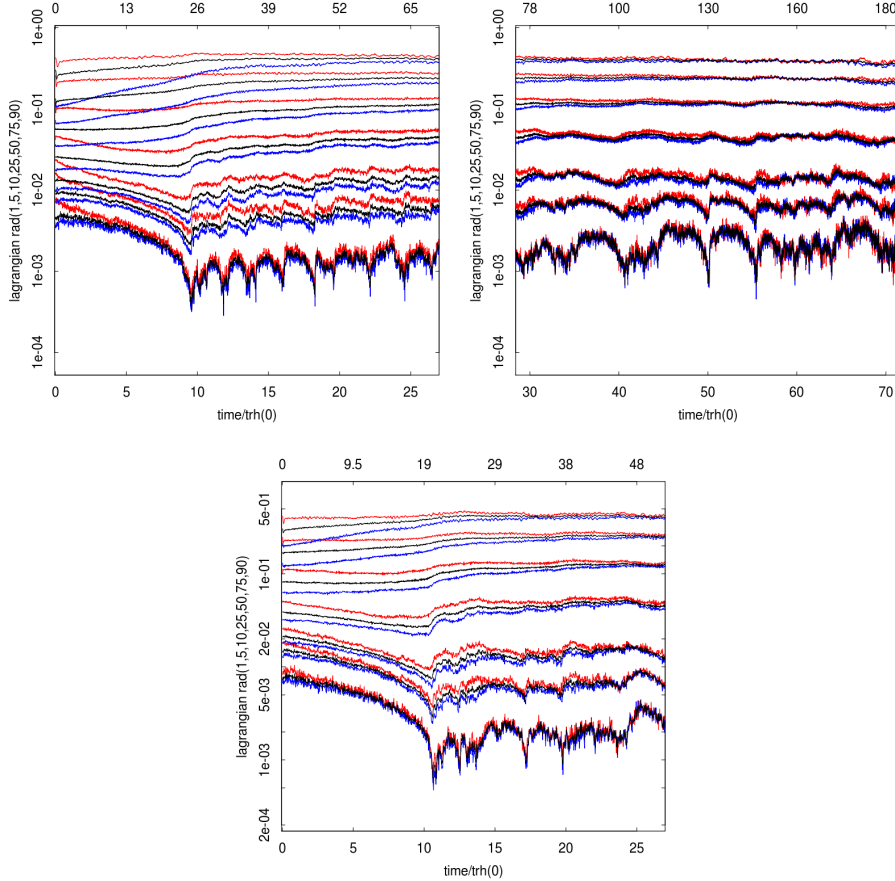
All simulations start with a total number of particles  $N = 10,000$ ; initially the numbers of FG and SG particles are equal. We assume that the cluster is tidally truncated and therefore that the King truncation radius is equal to the cluster Jacobi radius,  $R_J$ . Particles are removed from the simulation after reaching a radius equal to twice the Jacobi radius. As discussed in Section 1, the initial conditions adopted for our simulations refer to the possible structural properties of a multiple-population cluster after the early loss of FG stars.

To explore the role of the relaxation-driven evaporation of stars on the cluster structural and mixing properties, we also include a simulation with the same initial conditions as those of the *r25* system, but without a tidal field or tidal truncation, and in which stars were removed only after reaching a distance of about 1000 times the cluster half-mass radius. Hereafter we refer to this simulation as *r25isol*.

All simulations were run until the total mass of the system was 20 percent or less of its initial value. For the *r25isol* system, mass loss proceeds at a much slower rate and the simulation was stopped after the system had lost 20 percent of its initial mass. In order to explore the dependence of our results on the number of particles, two additional simulations with  $N = 30,000$  and  $N = 60,000$  particles were also run, with initial structural properties identical to those of the *r10* system.



**Figure 1.** Time evolution of the 1%, 5%, 10%, 25%, 50%, 75%, 90% lagrangian radii for SG stars (blue lines), FG stars (red lines) and all stars (black lines). The five rows of figures refer (from top to bottom) to the  $r25$ ,  $r25isol$ ,  $r10$ ,  $r5$ , and  $r2p5$  simulations. In each panel, time is expressed relative to the initial half-mass relaxation time of the entire system in the bottom horizontal axis, and to the initial half-mass relaxation time of the SG subsystem in the upper horizontal axis. In order to show more clearly the details of the lagrangian radius evolution, for each simulation (except for  $r2p5$ ) the left panels show only the evolution until  $\sim 25t_{rh}(0)$  and the right panels the rest of the evolution until the two populations are mixed.

Figure 1 – *continued*

### 3 RESULTS

#### 3.1 Dynamics of spatial mixing

We start the presentation of our results by focussing our attention on the dynamics of the spatial mixing process. We emphasize here that the simulations presented in this paper are aimed at understanding the fundamental aspects of the dynamics of multiple-population clusters; additional simulations currently in progress, including a spectrum of masses will allow us to more closely compare our theoretical results with observations. The panels of Fig.1 show the time evolution of the Lagrangian radii of the FG and SG populations (along with those of the entire system), and illustrate the system’s structural evolution and degree of spatial mixing. Overlap of all Lagrangian radii for the two populations indicates complete mixing. As indicated in Fig.1, the number of initial half-mass relaxation times (of the whole system or of the SG subsystem) needed to reach complete mixing of the two populations depends strongly on the initial concentration of the SG subsystem.

To illustrate the dynamics behind the mixing process and the role of relaxation-driven mass loss, Fig. 2 compares the time evolution of the ratio of the FG to the SG half-mass radii,  $R_{h,FG}/R_{h,SG}$ , a convenient measure of global mixing, for the *r25* and the *r25isol* runs. Initially, the ratio decreases relatively rapidly, as two-body relaxation acts to erase the initial spatial differences between the two pop-

ulations. However, its rate of change slows as the system evolves. The reason for this is that, after reaching core collapse (at  $t \sim 17t_{rh,SG}(0)$  for both the *r25* and the *r25isol* systems), the system enters its post-core collapse expansion phase. If the cluster did not lose a significant amount of mass during the expansion, its relaxation time would increase, with the half-mass radius and half-mass relaxation time growing with time as  $R_h \sim t^{2/3}$  and  $t_{rh} \sim t$  (see e.g. Spitzer 1987). We note that the same behavior, with the same implications for the mixing process, is expected no matter what mechanism (e.g. three-body binaries, primordial binaries, stellar evolution mass loss) drives the cluster expansion. (See e.g. Gieles et al. 2011 for a recent discussion of the role of mass loss due to stellar evolution in providing the energy needed to balance the energy flow from the cluster half-mass radius.)

The increasing relaxation time means that the evolution of any cluster property driven by two-body relaxation slows down accordingly. If we define the cluster dynamical age as  $\tau = \int_0^t dt/t_{rh}(t)$  and assume  $t_{rh} \sim t$ , it follows that, during this phase,  $\tau \sim \log t$  and the rate of the cluster dynamical aging slows down as  $d\tau/dt \sim 1/t$ . The decreasing rate of spatial mixing of the FG and SG populations evident in Fig. 2 is a manifestation of the decreasing cluster aging rate.

In reality, clusters lose mass, and the time evolution of  $t_{rh}$  and  $\tau$  deviate from the expressions derived on the assumption of zero mass loss. While the spatial mixing rate

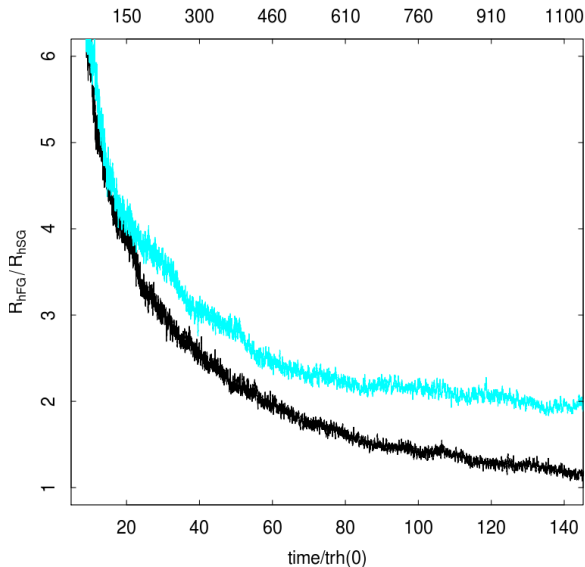


**Figure 2.** Time evolution of the ratio of the FG to the SG half-mass radii for the *r25* (black lower line) and the *r25isol* (cyan upper line) systems. Time is normalized to the initial half-mass relaxation time of the whole system in the lower axis, and to the initial half-mass relaxation time of the SG subsystem in the upper axis.

decreases with time for both the *r25* and the *r25isol* systems, Fig. 2 shows that the evolution of  $R_{h,FG}/R_{h,SG}$  for the *r25isol* system is significantly slower than for the *r25* system. This difference is due to the different mass loss rates of the two systems. As the amount of mass lost increases, the growth of the cluster relaxation time gradually slows, and eventually it starts to decrease, both as a result of the decreasing remaining mass and of the eventual contraction of the half-mass radius. As the cluster mass decreases so does its Jacobi radius, and the outer, less relaxed (and less mixed), layers are gradually stripped away. Thus, by enhancing the loss of less-mixed layers and slowing the growth of the cluster relaxation time, mass loss accelerates the cluster dynamical aging process and the evolution toward complete spatial mixing.

We further illustrate these points in Fig. 3. Here we focus on the local relaxation time  $t_{relax}(r) = 0.34\sigma(r)^3/(G^2m\rho(r)\ln(0.11N))$ , which provides a more accurate measure of the level of mixing expected at different distances from the cluster center. Here,  $\sigma(r)$  is the cluster 1-D velocity dispersion,  $\rho(r)$  the cluster mass density and  $N$  is the total number of stars. Fig. 3 shows the time evolution of the local cluster dynamical age  $\tau(r, t) = \int_0^t dt/t_{relax}(r, t)$  at different distances from the cluster center. The slowdown in the time evolution of  $\tau$  when the cluster expansion starts (marked by the vertical dotted line) and the differences between the dynamical aging of the *r25* and the *r25isol* systems are evident in this figure.

Fig. 3 also shows the radial dependence of the cluster dynamical age: as expected,  $\tau(r, t)$  decreases at larger distances from the cluster center, and the cluster outer regions mix on longer time scales than the inner regions. The implications of this radial variation of the dynamical age on

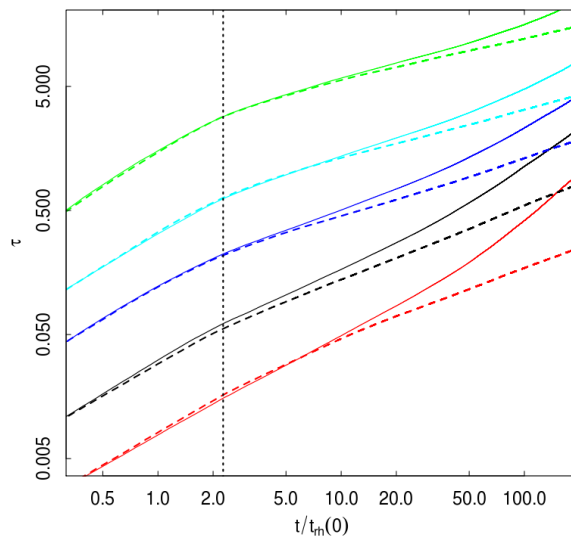


**Figure 3.** Time evolution of the cluster dynamical age  $\tau$  (see text for definition) for the *r25* (solid lines) and the *r25isol* (dashed lines) systems. The five lines for each system refer (from top to bottom) to the values of  $\tau$  measured at the 25%, 40%, 50%, 60%, 75% lagrangian radii. The vertical dotted line marks the time of core collapse (see also the top left panel of Fig. 1).

the mixing process, and its imprint on the radial variation of the fraction of SG stars, are discussed in more detail in Section 3.4.

The general evolution toward spatial mixing is therefore driven by internal two-body relaxation and accelerated by mass loss. The mass loss rate due to two-body relaxation is determined primarily by the strength of the external tidal field (see e.g. Vesperini & Heggie 1997, Baumgardt & Makino 2003, Gieles & Baumgardt 2008), while the local internal relaxation rate is determined by the cluster structural properties and their radial variation within the cluster. The different processes (and time scales) involved in the mixing dynamics imply that, in general, it is not possible to determine a universal mixing time scale simply in terms of the cluster initial half-mass relaxation time scale. The *r25* and *r25isol* systems share the same initial structure but, after a given number of initial half-mass relaxation time scales, because of their different mass loss history, they have reached a significantly different degree of mixing.

### 3.2 Dependence on the SG initial concentration

We have carried out a set of four simulations with different SG initial spatial concentrations. In comparing the evolution of these systems, we assume they represent clusters with the same initial masses and tidal radii (equal to the Jacobi radius), but different internal structures determined by the concentration of the SG population. As shown in numerous investigations based on Fokker-Planck and N-body simulations (see e.g. Chernoff & Weinberg 1990, Vesperini & Heggie 1997, Baumgardt & Makino 2003, Gieles & Baumgardt 2008), systems with the same tidal radius and mass share a similar relaxation-driven dissolution time scale, with only

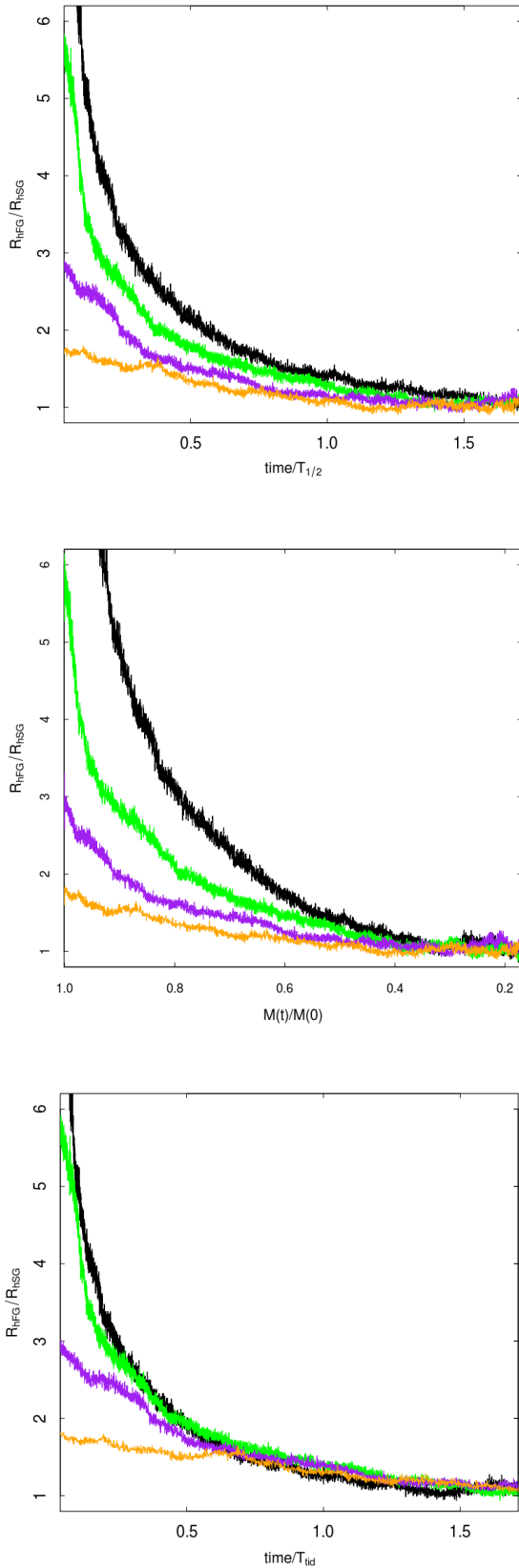


**Figure 4.** Evolution of  $R_{h,FG}/R_{h,SG}$  as a function of time normalized to the half-mass lifetime of each cluster,  $T_{1/2}$  (top panel), the ratio of the cluster mass to the initial mass (middle panel), and time normalized to a common reference time  $T_{tid} = 0.1N^{0.65}/\omega$  (lower panel; see Section 3.2 for a discussion of  $T_{tid}$ ). The lines in each panel refer to the *r25* (black), *r10* (green), *r5* (purple), and the *r2p5* (orange) systems.

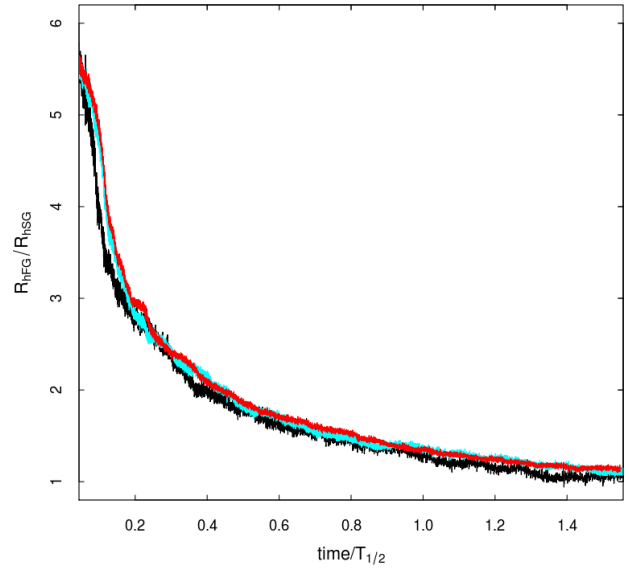


**Figure 5.** Evolution of  $R_{h,FG}/R_{h,SG}$  as a function of time normalized to  $T_{1/2}$  for the *r10* system with (from top to bottom)  $N = 60,000$  (top red line),  $N = 30,000$  (middle cyan line), and  $N = 10,000$  (lower black line).

a weak dependence on the internal structure of the cluster (see e.g. Gieles & Baumgardt 2008). The four systems investigated here span almost an order of magnitude in initial half-mass relaxation time, but only a factor of two in the half-mass lifetime (defined as the time needed to lose half of their initial mass due to the effects of two-body relaxation). The upper and middle panels of Fig. 4 show the evolution of  $R_{h,FG}/R_{h,SG}$  as a function of time normalized to each cluster’s half-mass time scale,  $T_{1/2}$ , and as a function of the cluster total mass (normalized to its initial value).

The lower panel of Fig. 4 shows  $R_{h,FG}/R_{h,SG}$  as a function of time normalized to a common reference time,  $T_{tid}$ , defined as  $T_{tid} = 0.1N^{0.65}/\omega$ , where  $\omega = \sqrt{GM/3R_j^3}$ . The definition of  $T_{tid}$  follows from studies showing that this functional form provides a good fit to the scaling of the relaxation-driven tidal dissolution (or half-mass) time scale with initial cluster properties. The exact value of the numerical factor needed for  $T_{tid}$  to match half-mass time scale depends on the cluster mass spectrum and the cluster structure (see e.g. Gieles & Baumgardt 2008 for a discussion on the dependence on the latter). Note that  $T_{tid}$  is closely related to the dynamical family parameter introduced by Chernoff & Weinberg 1990 (see their Table 3).

As just discussed, both internal two-body relaxation and (indirectly) mass loss drive the evolution of the FG-SG mixing. Despite the initial differences in the SG concentration, all systems approach a state of complete mixing ( $R_{h,FG}/R_{h,SG} \sim 1$ ) after approximately the same number of  $T_{1/2}$  and  $T_{tid}$  time scales, and after losing 60–70 percent of their mass.

Fig. 5 compares the evolution of  $R_{h,FG}/R_{h,SG}$  as a function of  $t/T_{1/2}$  for clusters with the structure of the *r10*

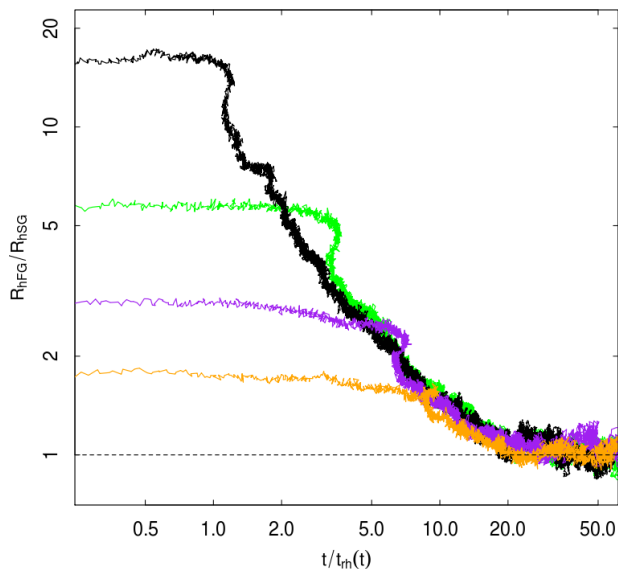


**Figure 6.** Evolution of  $R_{h,FG}/R_{h,SG}$  as a function of time  $t$  relative to the instantaneous cluster half-mass relaxation time scale  $t_{rh}(t)$ , calculated using the 3D half-mass radius,  $R_h$ . The lines refer to the  $r25$  (black),  $r10$  (green),  $r5$  (purple), and the  $r2p5$  (orange) systems.

system but different values of  $N$ . The time evolution of  $R_{h,FG}/R_{h,SG}$  shows only a very weak dependence on  $N$ .

### 3.3 Connection between SG/FG mixing and $t/t_{rh}(t)$

While, as pointed out at the beginning of this section, the goal of the simulations presented in this paper is to understand the fundamental aspects of multiple-population cluster dynamics and not to directly compare the results of simulations with observations, we nonetheless think it is important to identify those parameters that can be most easily measured for real clusters and might be correlated with the degree of SG/FG mixing.

One observable quantity that can be reliably estimated for all clusters is the current half-mass relaxation time,  $t_{rh}(t)$ . In Fig. 6 we show the evolution of the degree of mixing (as measured by  $R_{h,FG}/R_{h,SG}$ ) versus the ratio  $t/t_{rh}(t)$ . This figure suggests that  $t/t_{rh}(t)$  may be a good observational indicator of the extent to which a cluster still retains memory of the initial SG segregation.

It is important to recognize from Fig. 6 that, when interpreting cluster-to-cluster differences in the current SG–FG mixing state, one must also consider possible differences in the initial degree of SG concentration. For example, two clusters starting with initial conditions similar to our  $r25$  and  $r5$  simulations might be characterized by different relative SG–FG spatial distributions even if observed at the same dynamical phase and after having lost the same amount of mass (see Fig. 4). Observations of clusters thought to be at the same dynamical phase may thus shed

light on the extent of the differences in the initial structural properties and concentration of the SG subsystem.

### 3.4 Spatial mixing and the radial variation of the FG–SG number ratio

As shown in Figs. 1, the FG–SG mixing process occurs more efficiently and on a shorter time scale in the cluster inner regions, where the local two-body relaxation time scale is shorter. In this section we explore further the evolution of the radial dependence of the mixing process.

Fig. 7 shows the radial profiles of the number ratio of SG to FG stars  $N_{SG}/N_{FG}$  for the  $r10$  system at different stages of its evolution (the evolution of the other systems shown in this figure is representative of the other systems investigated). The system starts with the SG population concentrated in the innermost regions; as the cluster evolves and the FG and SG stars mix, the inner flat portion of the  $N_{SG}/N_{FG}$  profiles progressively extends toward the outer regions. Complete mixing corresponds to a flat profile extending over the entire cluster.

During the evolution the  $N_{SG}/N_{FG}$  radial profile is characterized by an approximately flat inner region followed by a declining outer portion corresponding to regions increasingly dominated by FG stars. In the outer regions, the  $N_{SG}/N_{FG}$  profile is characterized again by an approximately flat portion followed, in some cases, by a weak final rise in the profile in the cluster outermost regions.

As our simulations show, during a large fraction of a cluster evolution, the SG and the FG populations are not completely mixed and  $N_{SG}/N_{FG}$  varies with the distance from the cluster center. This fact has several implications: First, some memory of the initial SG segregation predicted by D’Ercole et al. (2008) should still be preserved and observable in many clusters today. Second, the observational determination of the SG-to-FG number ratio at a given distance from the center of a cluster will, in general, differ from the global value of that quantity [hereafter we will refer to the global value of  $N_{SG}/N_{FG}$  as  $(N_{SG}/N_{FG})_{glob}$ ]. Third, when exploring cluster-to-cluster differences in the SG-to-FG number ratio, we must take into account the possibility that part of these differences might arise if observations cover different radial zones of different clusters, relative to the half-mass radius.

The global SG-to-FG number ratio and its cluster-to-cluster variation are key ingredients of, and constraints on, our ability to understand and model the formation and evolution of multiple populations in globular clusters. It is therefore important to properly understand the relationship between the observational estimates of the SG-to-FG number ratio and its actual global value.

Fig. 8 shows the time evolution of the radius,  $R_{glob}$ , at which the local value of  $N_{SG}/N_{FG}$  equals the global value  $(N_{SG}/N_{FG})_{glob}$ . The evolution of  $R_{glob}$  is shown only until  $t/T_{1/2} \sim 1$  since, beyond this time, as the system approaches complete mixing  $R_{glob}$  becomes very noisy and not well defined. Fig. 8 shows that  $N_{SG}/N_{FG}$  generally equals  $(N_{SG}/N_{FG})_{glob}$  at radii  $\sim (1-2)R_h$ . These results provide a first approximate indication of the range of radial distances to be targeted in observational studies in order to estimate the global SG-to-FG number ratio from observations covering only a limited radial range. Additional simulations with

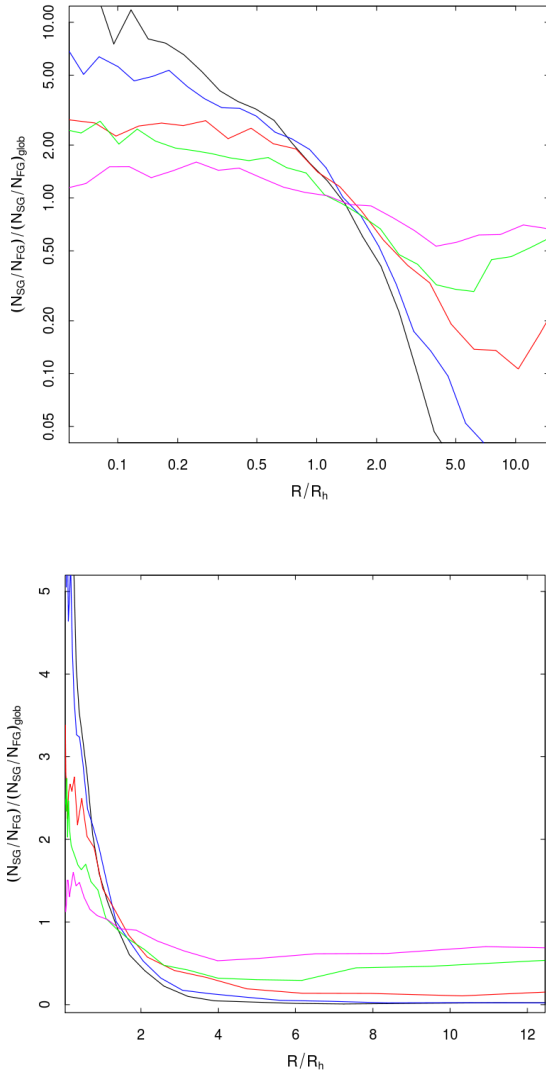


**Figure 7.** Evolution of the radial profile of  $N_{SG}/N_{FG}$  for the  $r10$  system. Radius is normalized to the instantaneous half-mass radius, and  $N_{SG}/N_{FG}$  is normalized to the global SG-to-FG number ratio. In each panel the profiles are shown at  $t/t_{rh}(0)$  [and  $t/T_{1/2}$ ,  $t/t_{rh}(t)$ ] approximately equal to 0.2 (0.003, 0.2) (black), 1 (0.015, 1) (blue), 5 (0.08, 3.5) (red), 15 (0.23, 5) (green line), and 45 (0.7, 10) (magenta). The top panel shows the profiles with a log-log scale to highlight the inner structure while the lower panel shows the same profiles in linear scale to highlight the outer regions.

a spectrum of masses are currently underway, and will allow a refined estimate of  $R_{glob}$  and more direct comparisons with observations.

### 3.5 Evolution of the global SG-to-FG number ratio

As shown by D’Ercole et al. (2008), the transition from a cluster initially dominated by FG stars to one with similar numbers of SG and FG stars (or even dominated by SG stars) occurs mainly during the cluster’s early evolu-

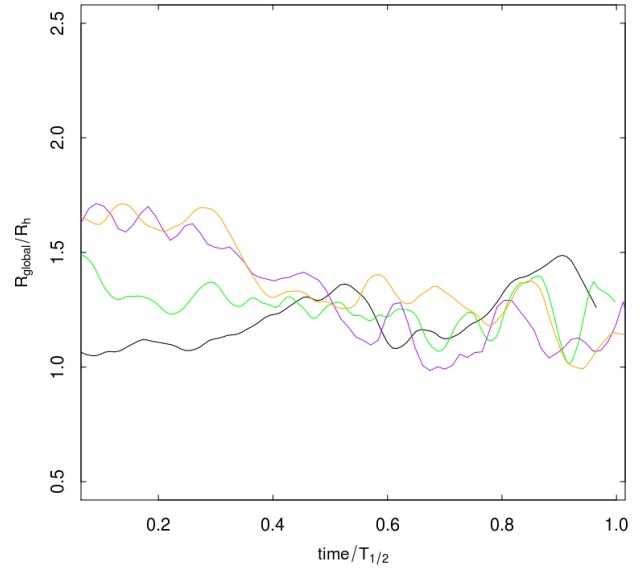


**Figure 8.** Time evolution of the ratio of the radius  $R_{glob}$ , at which the local value of  $N_{SG}/N_{FG}$  equals the global value  $(N_{SG}/N_{FG})_{glob}$ , to the cluster half-mass radius,  $R_h$ . Black, green, purple and orange lines refer, respectively, to the  $r25$ ,  $r10$ ,  $r5$ , and  $r2p5$  simulations.

tion. This transition is due to the loss of FG stars during the cluster’s early expansion triggered by the loss of SNII ejecta.

During the subsequent long-term evolution, mass loss due to two-body relaxation removes both FG and SG stars from the cluster. Until the two populations are completely mixed, two-body relaxation will still lead to a slight preferential loss of FG stars and further increase the SG-to-FG number ratio (although this increase is much smaller than that during the cluster early evolution; see D’Ercole et al. 2008). Fig. 9 shows the time evolution of the global SG-to-FG number ratio,  $(N_{SG}/N_{FG})_{glob}$ . For the systems studied here, during the long-term evolution  $(N_{SG}/N_{FG})_{glob}$  increases by only a factor of  $\sim 1.3 - 1.4$ .

If stars with chemical properties typical of observed SG populations can form only in globular clusters, the SG stars observed in the Galactic halo (see e.g. Martell & Grebel 2010, Carretta et al. 2010b) must have been lost by clusters mainly during the long-term evolution phase explored in this paper. As discussed by Vesperini et al. (2010; see also Carretta et al. 2010b, Schaerer & Charbonnel 2011), the fraction of SG stars in the Galactic halo is a very important quantity that can shed light on the connection between globular clusters, their formation and dynamical history, and their contribution to the assembly of the Galactic halo.

## 4 DISCUSSION AND CONCLUSIONS

Our previous study of the formation and evolution of multiple populations (D’Ercole et al. 2008) showed that SG stars form in the innermost regions of a cluster initially dominated



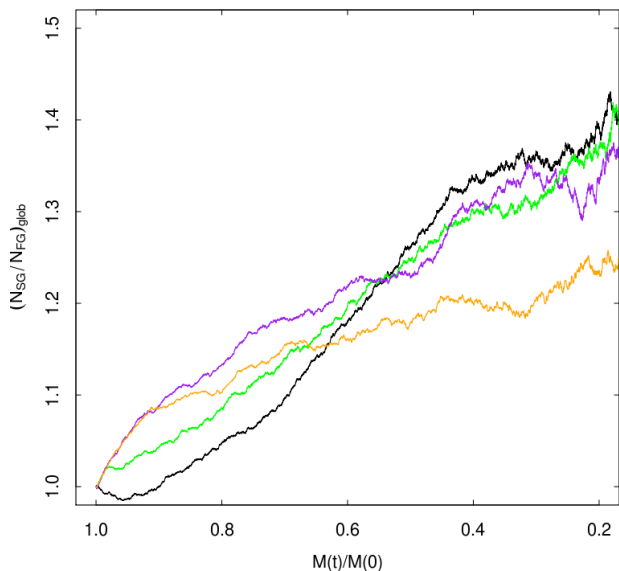


**Figure 9.** Time evolution of  $(N_{SG}/N_{FG})_{glob}$  for the simulations  $r25$  (black),  $r10$  (green),  $r5$  (purple),  $r2p5$  (orange).

by FG stars. Following the early cluster expansion triggered by mass loss due to SNII, a large fraction of FG stars escape the cluster, leaving a system with comparable numbers of FG and SG stars, with the SG stars strongly segregated near the cluster center. The simulations presented here follow the subsequent long-term evolution of these clusters, driven by two-body relaxation. By means of a survey of N-body simulations, we have investigated the dynamical evolution of multiple-population clusters, focusing our attention on cluster structural evolution and the FG-SG mixing process. We have studied initial conditions characterized by different degrees of the initial concentration of the SG subsystem.

Two-body relaxation is the key process driving the mixing of the two populations. As the local two-body relaxation time scale increases in the cluster outer regions, this process becomes less efficient at larger distances from the cluster center. Moreover, as soon as an energy source in the cluster core causes a cluster to start expanding, the cluster relaxation time increases with time and the rate of its dynamical aging increasingly slows down. A significant slowdown in the evolution toward complete mixing ensues (see Figs. 2 and 3).

Our simulations show that as cluster evolution continues, relaxation-driven mass loss affects the mixing process by slowing and eventually reverting the growth of the cluster relaxation time, and by causing the loss of the cluster’s outer unmixed layers. By comparing the evolution of clusters with the same initial structure but different mass-loss rates, we have quantified this process and illustrated the joint role of internal relaxation and tidal mass loss in the evolution toward complete mixing. Our simulations imply that, unless a cluster has lost a significant fraction of its mass ( $\gtrsim 60 - 70\%$ ; as discussed in the paper, we refer here to the mass lost during the cluster long-term evolution, and not to the early loss of FG stars), FG-SG mixing will not

be complete and the SG stars will be centrally concentrated relative to the FG population (see Fig. 4).

To further explore the radial dependence of the mixing process, we have followed the time evolution of the radial profile of the SG-to-FG number ratio,  $N_{SG}/N_{FG}$  (see Fig. 7). We have shown that as SG-FG mixing proceeds, the  $N_{SG}/N_{FG}$  profile can be divided into three different regions: (1) an inner region where  $N_{SG}/N_{FG}$  is flat; (2) an intermediate region where the FG is increasingly dominant, with  $N_{SG}/N_{FG}$  declining with increasing radius; (3) an outer region where the  $N_{SG}/N_{FG}$  profile flattens (the outermost cluster regions are in some cases characterized by a slightly rising  $N_{SG}/N_{FG}$  profile).

Since, as discussed above, reaching complete mixing (and therefore a flat  $N_{SG}/N_{FG}$  radial profile) requires the cluster to be in an advanced phase of dynamical evolution, with the loss of a significant fraction of stars, we expect that a  $N_{SG}/N_{FG}$  profile characterized by the regions described above will be found in all clusters which have not undergone strong relaxation-driven mass loss—possibly a large fraction of the Galactic globular cluster population. Although a detailed and quantitative comparison with observations is beyond the scope of the analysis carried out in this paper, our study provides a preliminary indication of the link between the level of SG/FG mixing and parameters that can be determined observationally for real clusters. Specifically, we have illustrated the relation between SG/FG mixing and the ratio  $t/t_{rh}(t)$  (see Fig.6).

A few observational studies have explored the differences in the spatial distribution of FG and SG stars in globular clusters, and find that, in agreement with the prediction of the formation and evolution models presented in D’Ercole et al. (2008) and the results presented in this paper, SG stars do tend to be concentrated in the cluster inner regions (Bellini et al. 2009, Carretta et al. 2010a, Lardo et al. 2011, Kravtsov et al. 2010, 2011 Nataf et al. 2011, Johnson & Pilachowski 2012, Milone et al. 2012). It is interesting to note the similarity between the overall shape of the  $N_{SG}/N_{FG}$  profile found in our simulations and the observational profiles as presented in Lardo et al. (2011), Bellini et al. (2009), and Milone et al. (2012). It is interesting to point out that all these clusters have values of  $t/t_{rh}(t)$  (assuming a common age of  $t = 11.5$  Gyr and  $t_{rh}$  calculated from the Harris (1996, 2010 edition) catalogue, taking into account the approximate relation between the 2D half-mass radius  $R_{h,2D}$ , and the 3D half-mass radius  $R_h$ ,  $R_h \simeq \frac{4}{3}R_{h,2D}$ ) such that the presence of a radial gradient in the  $N_{SG}/N_{FG}$  profile is expected, and in agreement with the simulations presented in this paper (see Fig.6).

Unless a cluster is completely mixed, the SG-to-FG number ratio determined from observations at a given distance from the cluster center is in general different from the global value. This implies that care must be used in comparing the SG-to-FG number ratio in different clusters: if different clusters are observed at different distances from the center, cluster-to-cluster differences in this number might be found even for systems with the same  $(N_{SG}/N_{FG})_{glob}$ . Our simulations indicate that, so long as mixing is not complete, the local value of  $N_{SG}/N_{FG}$  measured at  $R \approx (1 - 2)R_h$  is approximately equal to the global SG-to-FG number ratio.

**ACKNOWLEDGMENTS**

E.V. and S.M. were supported in part by grants NASA-NNX10AD86G and HST-AR-12158.01, HST-AR-12158.05. F.D. and A.D. acknowledge support from grant PRIN-INAF 2011 'Multiple populations in Globular Clusters: their role in the Galaxy assembly'. We would like to thank M. Bellazzini and C. Lardo for useful discussions.

**REFERENCES**

- Baumgardt H., Makino, J., 2003, MNRAS, 2003, 340, 227  
 Bekki, K., 2011, MNRAS, 412, 2241  
 Bellini, A., et al. 2009, A&A, 507, 1393  
 Carretta, E., et al. 2009a, A&A, 505, 117  
 Carretta, E., Bragaglia, A., Gratton, R., Lucatello, S. 2009b, A&A, 505, 139  
 Carretta, E., Bragaglia, A., D'Orazi, V., Lucatello, S., Gratton, R. G., 2010a, A&A, 519, A71  
 Carretta, E., et al. 2010b, A&A, 516, A55  
 Chernoff, D.F., Weinberg, M.D., 1990, ApJ, 351, 121  
 Cottrell, P. L.; Da Costa, G. S., 1981, ApJ, 245, L79  
 D'Antona, F., Caloi, V., Montalbán, J., Ventura, P., Gratton, R. 2002, A&A 395, 69  
 D'Antona F., Caloi V., 2004, ApJ, 611, 871  
 D'Antona, F., Caloi, V. 2008, MNRAS, 390, 693  
 Decressin, T., Meynet, G., Charbonnel, C., Prantzos, N., Ekström, S. 2007, A&A, 464, 1029  
 Decressin, T., Baumgardt, H., Kroupa, P., 2008, A&A, 492, 101  
 Decressin, T., Baumgardt, H., Charbonnel, C., Kroupa, P., 2010, A&A, 516, A73  
 de Mink, S.E., Pols, O.R., Langer, N., Izzard, R.G., 2009, A&A, 507, L1  
 D'Ercole, A., Vesperini, E., D'Antona, F., McMillan, S. L. W., Recchi, S., 2008, MNRAS, 391, 825  
 D'Ercole, A., D'Antona F., Ventura P., Vesperini E., McMillan S.L.W., 2010, MNRAS, 407, 854  
 D'Ercole, A., D'Antona F., Carini, R., Vesperini, E., Ventura P., 2012, MNRAS, 423, 1521  
 Dupree, A. K., Strader, J., Smith, Graeme H., 2011, ApJ, 728, 155  
 Gaburov, E., Harfst, S., Portegies Zwart, S., 2009, *New Astron.*, 14, 630  
 Gieles, M., Baumgardt, H., 2008, MNRAS, 389, L28  
 Gieles, M., Heggie, D.C., Zhao, H., 2011, MNRAS, 413, 2509  
 Gratton, R., Carretta, E., Bragaglia, A., 2012, *A&ARv*, 20, 50  
 Harris, W.E. 1996, AJ, 112, 1487  
 Johnson C. I., Pilachowski C. A., 2012, ApJ, 754, L38  
 King, I.R., 1966, AJ, 71, 64  
 Kravtsov, V., Alcano, G., Marconi, G., Alvarado, F., 2010, A&A, 512, L6  
 Kravtsov, V., Alcano, G., Marconi, G., Alvarado, F., 2011, A&A, 527, L9  
 Lardo, C., Bellazzini, M., Pancino, E., Carretta, E., Bragaglia, A., Dalessandro, E., 2011, A&A, 525, A114  
 Makino, J., Fukushige, T., Koga, M., Namura, K., 2003, *PASJ*, 551, 1163  
 Martell, S.L., Grebel, E.K., 2010, A&A, 519, A14  
 Milone, A.P., et al., 2012, ApJ, 744, 58  
 Nataf, D.M., Gould, A., Pinsonneault, M. H., Stetson, P. B., 2011, ApJ, 736, 94  
 Pasquini, L., Mauas, P., Käuffl, H. U., Cacciari, C., 2011, A&A, 531, A35  
 Portegies Zwart, S., McMillan, S. L. W., Hut, P., Makino, J., 2001, MNRAS, 321, 199  
 Piotto G. et al., 2007, ApJ, 661, L53  
 Renzini, A., 2008, MNRAS, 391, 354  
 Schaerer, D., Charbonnel, C., 2011, MNRAS, 413, 2297  
 Spitzer, L., 1987, *Dynamical Evolution of Globular Clusters*, (Princeton: Princeton University Press)  
 Ventura, P., D'Antona, F., Mazzitelli, I., Gratton, R., 2001, ApJ, 550, L65  
 Vesperini, E., Heggie, D.C., 1997, MNRAS, 289, 898  
 Vesperini, E., McMillan, S. L. W., D'Antona, F., D'Ercole, A., 2010, ApJ, 718, L112  
 Vesperini, E., McMillan, S. L. W., D'Antona, F., D'Ercole, A., 2011, MNRAS, 416, 355